Video Article

A 3D-printed Chamber for Organic Optoelectronic Device Degradation Testing

Emma Mogus[1], Benjamin Torres-Kulik[1], Christopher Gustin[2], Ayse Turak[1]

[1]Department of Engineering Physics, McMaster University

[2]Department of Physics, Engineering Physics and Astronomy, Queen's University

Correspondence to: Ayse Turak at turaka@mcmaster.ca

URL: https://www.jove.com/video/56925
DOI: doi:10.3791/56925

Keywords: Engineering, Issue 138, Organic electronics, degradation testing, additive manufacturing, humidity testing, semiconductor parameterization, perovskite solar cells, organic light-emitting diodes

Date Published: 8/10/2018

Citation: Mogus, E., Torres-Kulik, B., Gustin, C., Turak, A. A 3D-printed Chamber for Organic Optoelectronic Device Degradation Testing. *J. Vis. Exp.* (138), e56925, doi:10.3791/56925 (2018).

Abstract

In this manuscript, we outline the manufacture of a small, portable, easy-to-use atmospheric chamber for organic and perovskite optoelectronic devices, using 3D-printing. As these types of devices are sensitive to moisture and oxygen, such a chamber can aid researchers in characterizing the electronic and stability properties. The chamber is intended to be used as a temporary, reusable, and stable environment with controlled properties (including humidity, gas introduction, and temperature). It can be used to protect air-sensitive materials or to expose them to contaminants in a controlled way for degradation studies. To characterize the properties of the chamber, we outline a simple procedure to determine the water vapor transmission rate (WVTR) using relative humidity as measured by a standard humidity sensor. This standard operating procedure, using a 50% infill density of polylactic acid (PLA), results in a chamber that can be used for weeks without any significant loss of device properties. The versatility and ease of use of the chamber allows it to be adapted to any characterization condition that requires a compact-controlled atmosphere.

Video Link

The video component of this article can be found at https://www.jove.com/video/56925/

Introduction

Organic and perovskite optoelectronic devices, solar cells, and light-emitting diodes based on π-conjugated semiconducting organic molecules and organometal halides are a rapidly growing field of research. Organic light-emitting diodes (OLEDs) are already a major technological element in lighting and displays[1], and organic photovoltaics have begun to achieve efficiencies that make them competitive with amorphous silicon[2]. The recent rapid advancement of perovskite-based devices for light absorbing and light-emitting applications[3,4,5] suggests that low-cost, easily processed devices are likely to soon find widespread deployment. However, all of these technologies suffer from a sensitivity to atmospheric contaminants, particularly moisture and oxygen, which limits their effective lifetimes[6,7,8,9].

For researchers studying such systems, it can be useful to have an adaptable, easy-to-use, portable, and reusable chamber to protect such sensitive materials or to expose them to contaminants in a controlled manner[10,11]. Though it is possible to use a glovebox for the characterization of air-sensitive devices, these large, expensive, and fixed-location, inert environments may be incompatible with the wide range of characterization that might be required. To provide a portable alternative, Reese *et al.*[10] proposed a small metal chamber based on a standard vacuum flange suitable for the electrical and optical characterization of organic devices. We have adapted this design, making it cheaper and more versatile by using 3D-printing to produce the chamber components. The use of 3D-printing, rather than machining, allows for rapid, cost-effective adjustments to changing sample or environmental requirements while maintaining the utility of the basic design. In this contribution, we outline the procedure to make such a chamber, and use it to extract the current-voltage characteristics of an organic diode device.

A good encapsulation of organic and perovskite devices should have WVTRs of 10^{-3} - 10^{-6} g/m^2/day for long-term device stability[12,13], to ensure little water ingress into the organic device even in very harsh conditions. As this chamber is designed to be a controlled environment for testing purposes rather than a long-term storage or encapsulation method, the requirements for an effective chamber are not as strict. The chamber should be able to maintain the device properties within a reasonable timeframe to perform characterization experiments. The standard operating procedure of using PLA results in a chamber which can be used for several days or even weeks with an incorporated gas flow, without a significant loss of the device properties.

Changing the materials, or even the shape and size of the chamber body can drastically affect the penetration of contaminants from the air into the chamber. Therefore, the ingress of moisture and oxygen needs to be carefully monitored for each design to determine the efficacy of the chamber. We, additionally to the fabrication of the chamber, outline a simple procedure for determining the WVTR of the chamber, using a commercially available humidity sensor, to establish a timeframe for the use of the chamber for experimentation.

Such a simple, yet versatile chamber allows for multiple types of experiments to be performed. They can act as inert atmosphere environments outside the glovebox, suitable for electrical and optical characterizations through the electrical feedthrough ports and window. Their portability

allows them to be used with standard electrical characterization equipment outside the lab where they were manufactured, which is useful in round robin testing for reliability[14] or to obtain certified measurements of the device performance[15]. These chambers are also particularly useful for studying the effects of the introduction of contaminants for controlled degradation tests, with simple modifications. The use of 3D printing allows a significant, rapid adaptability to changing device layouts, sizes, or testing requirements.

Protocol

1. The 3D Print Chamber Parts

Note: All printer preparation, “slicer” software settings, and print parameters were specific to the printer indicated in the **Table of Materials**. There is a wide array of 3D printers, each with their own set of preparation steps and optimal parameters. There is also a wide array of colors possible for the polymer filament used for the printed parts. It is not required to use the same plastic for each part.

1. Select the corresponding .stl files based on the desired chamber configuration.
   Note: These configurations are detailed in **Figure 1**, along with an exploded view of one complete chamber configuration.
2. Set up the slicing software to convert the .stl files to .gcode files that the printer will read.
   1. Download the slicing software listed in the **Table of Materials**.
   2. Select the printer in use by navigating to **Other** and find the printer in use.
   3. Navigate to **Settings** > **Printer** > **Manage Printers** > **Machine Settings** and change the settings as shown in **Figure 2**.
3. Convert the .stl file to a .gcode file with user-desired parameters with the slicing software.
4. Save the converted .gcode file to the SD card and insert it into the 3D printer.
5. Prepare the 3D printer for use.
   1. Cover the printing bed with blue masking tape. Ensure there are no rips, air bubbles, or uneven surfaces by running a credit card-type object over the surface.
   2. Level the printer bed if necessary. The method differs per printer and can be researched.
6. Navigate to **Print from SD card** on the 3D printer display and select the desired file.
   Note: The printer will, at first, heat up its bed and nozzle, and then the print will begin.
7. Repeat steps 1.3 - 1.6 for each part to be printed.

(a) **Chamber Configurations**

Chamber component	4 Pixel IV Test	6 Pixel IV Test	WVTR Test
Top Chamber	4Pixel_Top_Chamber.stl	6Pixel_Top_Chamber.stl	4Pixel_Top_Chamber.stl
	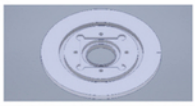	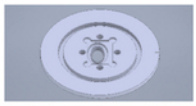	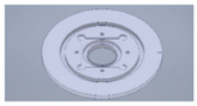
Retaining Ring	4Pixel_RetainingRing.stl	6Pixel_RetainingRing.stl	4Pixel_RetainingRing.stl
		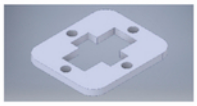	
Bottom Chamber	4Pixel_Bottom_Chamber.stl	6Pixel_Bottom_Chamber.stl	WVTR_Test_Bottom_Chamber.stl
	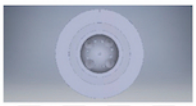		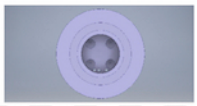
Bottom Chamber with Gas Flow Ports	4Pixel_GasFlow_Bottom_Chamber.stl	6Pixel_GasFlow_Bottom_Chamber.stl	N/A
	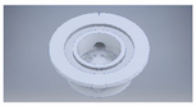		N/A

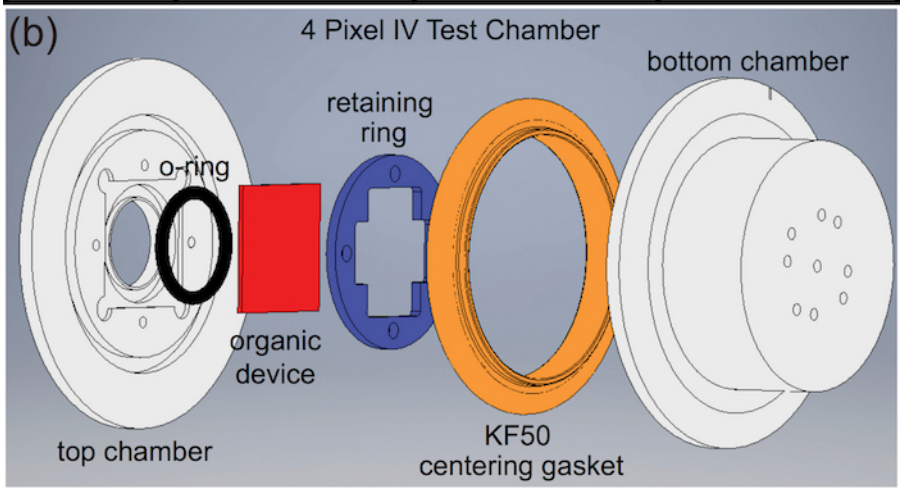

Figure 1: A configuration table with an exploded view of the test chamber. (**a**) This table shows the .stl files for various chamber configurations. The rows show 3D-rendered schematics of the variations on each chamber part to be printed. The columns show the necessary parts to complete a single chamber. Note that a chamber will have either a bottom chamber or a bottom chamber with gas ports, not both. (**b**) This panel shows an exploded CAD view of a printed chamber for a 4-pixel IV test configuration. Note that the O-ring, the organic device, and the KF50-centering gasket are not 3D printed. Please click here to view a larger version of this figure.

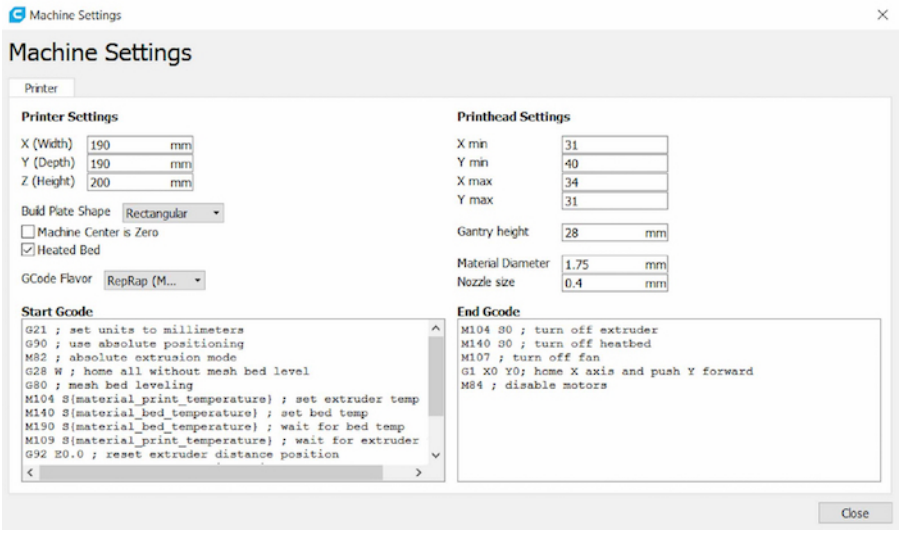

Figure 2: 3D printer settings. This is a screenshot of the required machine settings in the slicing software to produce the 3D-printed parts for the chambers. Please click here to view a larger version of this figure.

2. The Top Chamber Assembly

1. Add threaded inserts to top chamber (see **Figure 3b** for information on how to apply threaded inserts).
    1. Drill 4 tapping holes of 0.404 cm in diameter (size 21 imperial) to a depth of 0.397 cm (5/32 in) in the 4 pilot holes in the underside of the printed top chamber (see **Figure 1a**).
    2. Place a brass-tapered threaded insert with a #4-40 thread size (0.248 cm in diameter) into the drilled hole with the smaller diameter facing down.
    3. Turn on a soldering iron. When heated to around 330 - 350 °C, press the soldering iron tip to the threaded insert and apply nominal pressure as the insert heats the plastic to allow it to slide into the prepared holes. Keep applying pressure (ensuring the insert is moving straight down) until the top face of the insert and the underside face of the top chamber are about 1 mm apart.
    4. Lightly press the edge of a straightedge against the top face of the insert while the plastic is still hot to ensure it is flush with the underside face of the top chamber. Allow 1 min for the plastic to cool before continuing.
    5. Ensure the alignment of the inserts by placing the retaining ring over the insert and checking to see if the holes line up. See **Figure 3c**.
    6. Repeat the procedure of steps 2.1.2 - 2.1.5 for all 4 inserts.
2. Insert and press the size-116 butyl O-ring into the circular groove in the underside of the top chamber.
3. Place the organic device on top of the O-ring (see **Figure 4** for the details of 2 possible pixel patterns).
   Note: A single organic device can be made up of a number of individual diodes that can be measured independently. These are referred to as “pixels.” The patterns in **Figure 4** represent the orientation of the organic device as it should be placed in the top chamber. The notch on the side of the chamber should be to the left of the organic device (4-pixel) or below the organic device (6-pixel) (relative to the orientation marks on the patterns in **Figure 4**).
4. In a glovebox environment, fasten the retaining ring to the top chamber by screwing the four 4-40 thread screws (0.248 cm in diameter, 0.478 cm in length) through the retaining ring into the threaded inserts. Press the device between the retaining ring and the O-ring. Take extreme care not to crack the device by screwing the screws incrementally, going one-eighth turn each pass around.
   Note: To guarantee a sufficient seal, check that the O-ring is pressed against the device all around with a 15 - 25% compression.

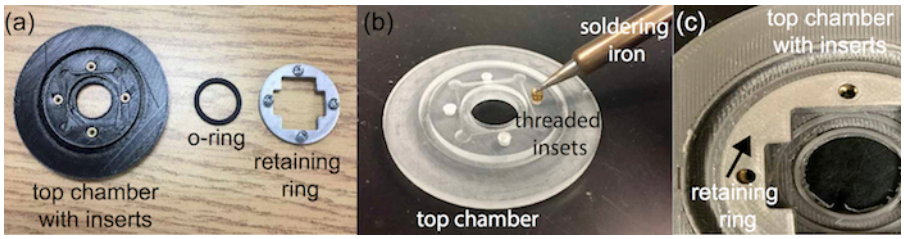

Figure 3: The assembling of the top chamber. (**a**) This panel shows a disassembled 4-pixel top chamber. (**b**) This panel shows the application of threaded inserts in the top chamber using a soldering iron. (**c**) This panel shows partially assembled top chamber components showing the alignment of the retaining ring to the top chamber (note that the O-ring and the screws are not shown for clarity). Different colors of PLA plastic were used for the printing of various parts; these have no effect on the performance of the chamber. Please click here to view a larger version of this figure.

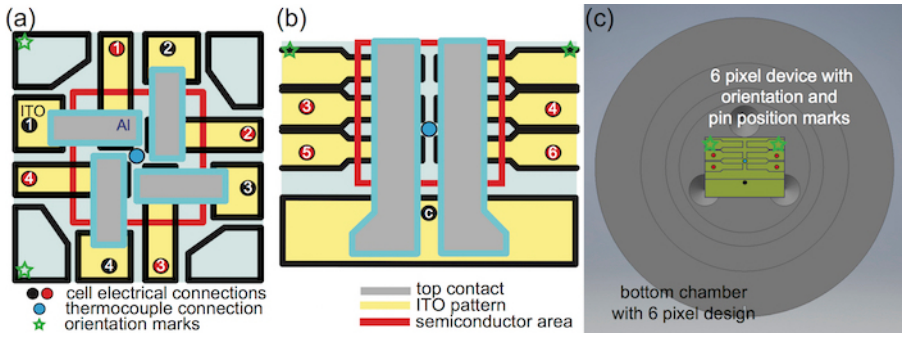

Figure 4: Possible device pixel patterns for a pin layout. These panels show the layout of the organic solar cell or light-emitting diode device used for designating the contact pin positions for (**a**) a 4-pixel and (**b**) a 6-pixel IV test chamber configuration. Each pixel is numbered with a reference to the orientation marks (green stars) for their correct placement in the chamber. Black and red circles represent the cathode and anode contacts (*i.e.*, pin positions), respectively. Note that for the 6-pixel configuration, the top two pixels are masked by the opening in the top chamber and not numbered as only four pixels can be tested under illumination or emission conditions. (**c**) This panel shows the orientation of a 6-pixel device relative to the 6-pixel bottom chamber with its pin positions indicated. Please click here to view a larger version of this figure.

5. Leave the assembled top chamber in a glovebox environment for ≥ 24 h to allow any moisture absorbed by the chamber to escape from the material. Continue with step 3 while waiting.

3. The Bottom Chamber Assembly

Note: Only follow step 3.1 if a configuration with a bottom chamber with gas flow ports is needed.

1. Add push-to-connect pneumatic connectors for an inert gas flow to the bottom chamber with gas flow ports (see **Figure 5**).
    1. Using a 1/8 in-sized National Pipe Thread (NPT) tap with a hand T-wrench, tap both holes located on the side of the bottom chamber with the gas flow ports. Ensuring that the hole to be tapped is vertical and the chamber is securely held in place, place the tap in the hole.
    2. Using the T-wrench attached to the tap, slowly twist the wrench clockwise, ensuring that the tap remains vertical and lined up with the hole as the threads are formed. Every 5 turns, twist the wrench counter-clockwise one full turn, and then twist another 5 turns, repeating until a thread is cut to the bottom of the hole.
    3. Wrap the Teflon tape around the 2-pneumatic push-to-connect connectors by wrapping the tape counter-clockwise around the threads (when viewing the fitting from above as it is screwed in) 2x.
    Note: For more information, please refer to a machinists' tapping guidebook.
    4. Screw the pneumatic connectors into the tapped holes, using a wrench to tighten them. Take care not to overtighten and crack the plastic.
    5. Apply low-pressure epoxy around the seated fittings. On a piece of foil, use a popsicle stick to mix 2-part base resin with 1-part hardener (both are included). This mixture is the epoxy.
    6. Using a toothpick, apply a layer of epoxy in and around the space between the bottom chamber with the gas flow ports and the fittings. Allow the epoxy to sit for 1 - 2 h for the resin to harden at 25 °C. For a full curing, allow the epoxy to rest for 24 h at 25 °C. Ensure that the set resin is white and solid when pressed.
    CAUTION: Epoxy hardener and epoxy resin cause burns and irritation of the eyes and skin. Epoxy may cause an allergic skin or respiratory reaction. It may cause respiratory tract irritation. It may be harmful if swallowed or absorbed through the skin. Ensure adequate ventilation and avoid any contact with skin and clothing. Do not breathe in the vapor. Wear eye protection and gloves when handling epoxy.
    7. Connect the pneumatic push-to-connect connectors with the manually operated push-to-connect valves with 2 cm pieces of Teflon tubing. The diameter of the tubing should match that which is required by the push-to-connect connector used.

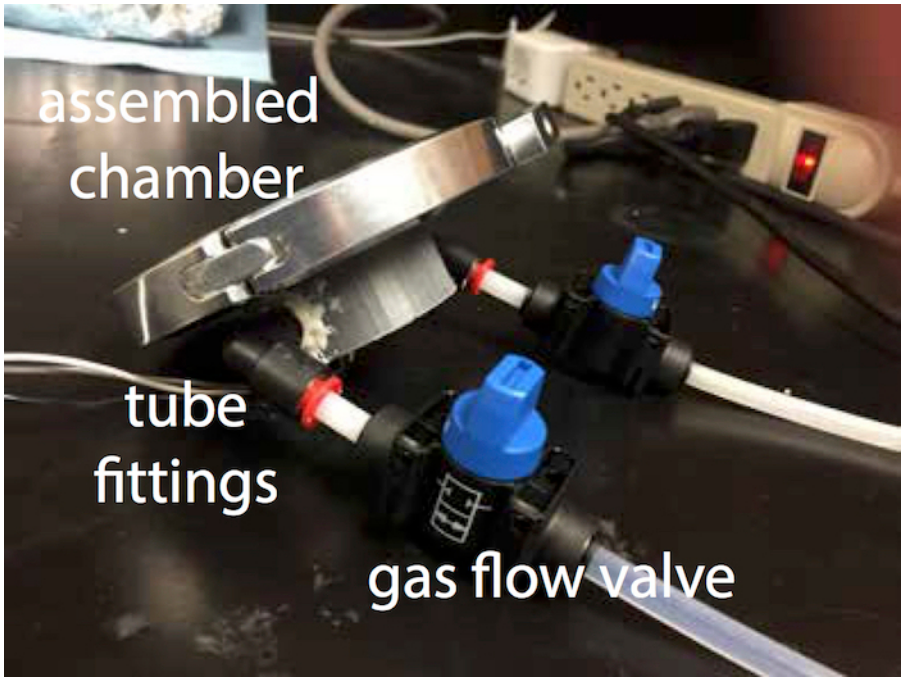

Figure 5: An assembled chamber with gas ports. This panel shows a fully assembled chamber including a bottom chamber with gas ports. The push-to-connect gas ports embedded in the available holes in the chamber are attached to tubing with gas flow control valves to control the introduction of gas. Note that the contact pins are omitted for clarity. Please click here to view a larger version of this figure.

2. Add electrical contact pins to the bottom chamber for a current voltage (IV) measurement (see **Figure 6**).
    1. Insert 6 - 7 mm of the narrow end of a pogo pin into the female end of a solder cup. The combination of these 2 parts is known as a contact pin. Using solder helping hands, suspend both parts of the contact pin horizontally.
    2. Turn on the soldering iron. When heated to around 330 - 350 °C, touch the iron to the connection region between the pogo pin and the solder cup.
    3. While still touching the iron to the area, press the solder to the connection region. If it has heated enough, the solder will melt. Ensure there is a thin layer of solder covering the area between the two parts all the way around the exterior of the contact pin. Ensure the solder is smooth with no bumps. See **Figure 6b**.
    4. Slide the contact pin into 1 of the holes in the underside of the bottom chamber. Slide the contact pin so that 2.2 cm of the solder cup end is protruding from the bottom of the bottom chamber.
    Note: The solder cup should stick out the bottom of the bottom chamber while the pogo pin should be towards the inside of the bottom chamber.
    5. For sealing, cover the region where the contact pin was inserted into the plastic with low-pressure epoxy suitable for vacuum applications. On a piece of foil, use a popsicle stick to mix 2-part resin with 1-part hardener until the mixture appears uniform.
    6. Using a toothpick, apply the epoxy around the contact pin and hole to eliminate the possibility of air ingress. Allow 1 - 2 h for the resin to harden at 25 °C. For a full curing, allow the epoxy to rest for 24 h at 25 °C. Ensure that the set resin is white and solid when pressed.
    CAUTION: Epoxy hardener and epoxy resin cause burns and irritation of the eyes and skin. Epoxy may cause an allergic skin or respiratory reaction. It may cause respiratory tract irritation. It may be harmful if swallowed or absorbed through the skin. Ensure adequate ventilation and avoid any contact with skin and clothing. Do not breathe in the vapor. Wear eye protection and gloves when handling epoxy.
    7. Repeat steps 3.2.1 - 3.2.6 to add the correct number of contact pins to the bottom chamber to fill the holes.

3. Place the assembled bottom chamber into a glovebox environment and leave it for at least 24 h.
Note: This is to allow any moisture absorbed by the chamber to escape from the material.

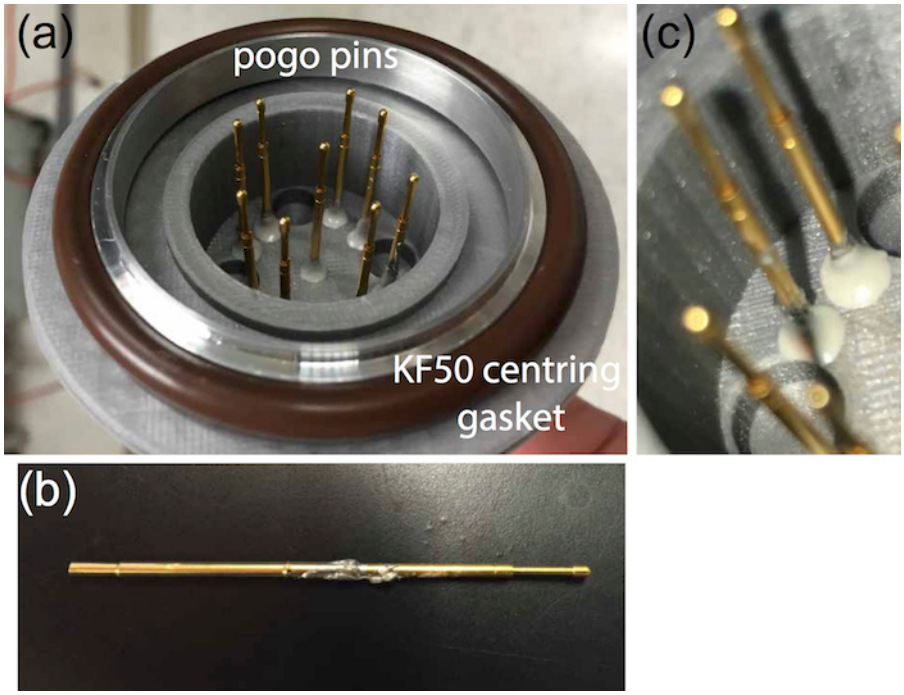

Figure 6: A complete, assembled bottom chamber. (**a**) This panel shows an assembled bottom chamber for a 4-pixel IV test configuration with the contact pins seated using low-pressure epoxy suitable for vacuum applications. The brown O-ring (KF50)-centering ring gasket is used to ensure a tight fitting with the top chamber. (**b**) This panel shows a solder cup and pogo pin after soldering. (**c**) This panel shows a close-up of set epoxy, showing the correct seating of the contact pin in the bottom chamber holes. Please click here to view a larger version of this figure.

4. The Final Assembly

Note: This assembly is to be done within a glovebox environment after both the assembled top and the bottom chamber have been inside the glovebox for ≥ 24 h.

1. Attach a KF50-centering gasket to the bottom chamber, as shown in **Figure 6**.
2. Place the top chamber on the bottom chamber, with the smooth side of the top chamber facing upwards and align the notches on both chamber parts to ensure proper contact with the organic device. See **Figure 1** for an exploded view of the whole chamber.
3. Secure the 2 chamber parts together using the KF50 clamp.
    1. Unfasten the wingnut on the clamp and place the clamp around the edge of the combined bottom chamber and top chamber.
    2. Using the inset of **Figure 7** for a clear representation, twist the wingnut as far as it can go to fasten the bolt, ensuring a tight seal around the 2 half-chambers. Leave the completed chamber in the glovebox until the software has been configured as detailed in step 5.

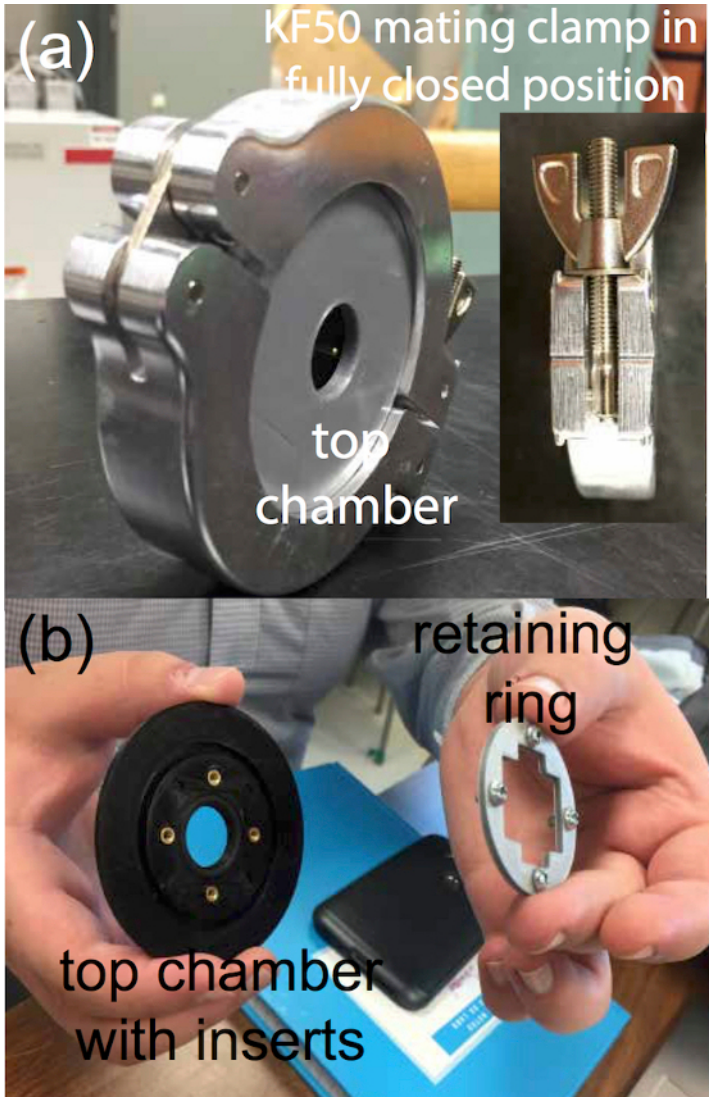

Figure 7: An assembled, complete test chamber. (**a**) This panel shows a fully assembled 4-pixel IV test chamber with a KF50 cast clamp ensuring a tight fit between the bottom and top chamber. The inset shows another angle of the KF50 clamp closed in the maximum tightness position. (**b**) This panel shows an assembly of the 4-pixel top chamber with the retaining ring (note that the O-ring is already mounted in the top chamber). Other chamber configurations are assembled in the same way. Please click here to view a larger version of this figure.

5. Conduct IV Measurements of the Individual Pixels on the Device

Note: This section details the procedure used to generate the data shown in the **Representative Results**. The source-measurement unit (SMU) and the Zero Insertion Force (ZIF) test board used are listed in the **Table of Materials**. However, any method of chamber connection to an SMU to collect current-voltage data can be used. All IV measurement steps were conducted on a Windows machine. “Pixel” refers to a single diode on the organic device.

1. Download and install the provided Python IDE.
2. Connect a BNC cable from the SMU 1 channel located on the SMU to the ZIF test board.
3. Connect the power supply to the SMU and connect it to a computer *via* a USB 2.0 cable.
4. Identify the correct COM port/serial port ID that corresponds to the connected SMU.
    1. For Windows devices, check which COM port corresponds to the connected SMU in the **Device Manager**. Take note of the COM number.
5. Open the **BasicIV.py** Python script.
6. Paste the COM port (Windows) in the indicated line of code in **BasicIV.py** as seen in **Figure 8**.
   Note: By default, the program will output data in the current working directory.

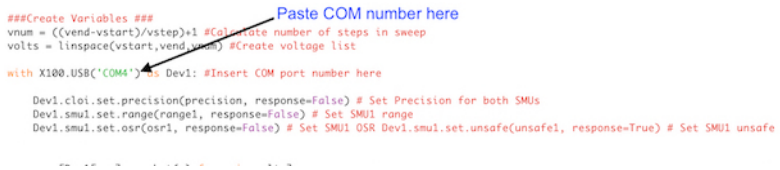

Figure 8: The IV measure in Python. This is a screen shot of the **BasicIV.py** Python script with the COM port location indicated. Please click here to view a larger version of this figure.

7. On the SMU, toggle the Range switch labeled “2” located near the SMU 1 channel to the **ON** position. See **Figure 9b**.
8. Remove the fully assembled chamber from the glovebox environment.
9. Bridge the connection between the contact pins and the ZIF test board using a method of choice (see **Figure 9**).
   Note: For this setup, a custom adaptor was made to bridge the connection between the contact pins and the ZIF test board when running IV measurements. This method can vary, as long as the connections are sufficient and add negligible resistance.
10. Switch the cathode pin to **Ground** and the anode pin to **BNC** for only 1 pixel at a time, ensuring the rest of them are switched **OFF**.
11. Run **BasicIV.py**.
    Note: When the measurement is completed, files of results and a plot of V_0 *versus* I_0 will be produced in the previously selected file path.
12. Repeat steps 5.10 and 5.11 for each pixel on the device using the pixel switches shown in **Figure 9** to measure the IV for each pixel.

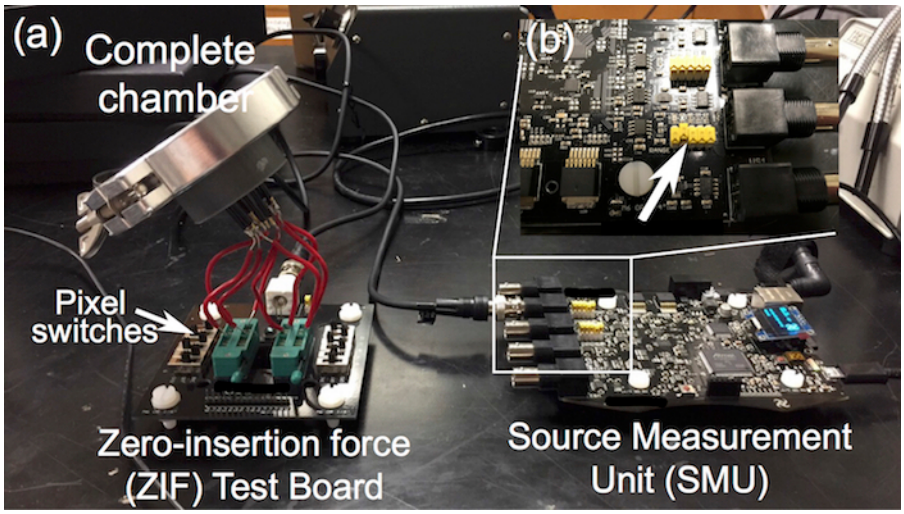

Figure 9: The IV measurement set-up. (**a**) This panel shows a fully assembled chamber connected to the zero-insertion force (ZIF) test board and source measurement unit (SMU) for an IV measurement testing. (**b**) This panel shows the range switch "2" set in the **ON** position to correctly connect the device to the SMU for the measurement. Please click here to view a larger version of this figure.

6. Assemble the Chamber for WVTR Testing

1. Add an internal humidity sensor to the WVTR test chamber for determining the WVTR.
   1. Solder 3 wires to the internal humidity sensor as shown in **Figure 10c**: 5 V (red), ground (green), and data (yellow). Ensure they are of sufficient length (approximately 15 cm).
   2. Feed internal humidity sensor wires through the holes at the bottom of the WVTR test bottom chamber.
   3. Using a toothpick, apply low-pressure epoxy around the wires inside and outside the bottom chamber as well as in any openings. On a piece of foil, use a popsicle stick to mix 2-part resin with 1-part hardener until the mixture appears uniform.
   4. Apply the epoxy around the wire and hole to eliminate the possibility of air ingress. Allow 1 - 2 h for the resin to harden at 25 °C. For a full curing, allow the epoxy to rest for 24 h at 25 °C. Ensure that the set resin is white and solid when pressed.
      CAUTION: Epoxy hardener and epoxy resin cause burns and irritation of the eyes and skin. Epoxy may cause an allergic skin or respiratory reaction. It may cause respiratory tract irritation. It may be harmful if swallowed or absorbed through the skin. Ensure adequate ventilation and avoid any contact with skin and clothing. Do not breathe in the vapor. Wear eye protection and gloves when handling epoxy.
2. Repeat step 2 to assemble a top chamber, replacing the device with a piece of glass the same size and thickness as the device that the chamber would be enclosing.
   Note: If a top chamber is already assembled, then it may be used for this purpose. Since no device is being measured, to mimic the conditions of a device, a piece of glass is used to seal the top chamber’s optical opening.
3. Leave the test bottom chamber, assembled top chamber, and KF50-centering ring unassembled in an oxygen-/moisture-free environment (glovebox) for 24 h to ensure an initial condition of 0% internal relative humidity.
4. Repeat step 4 to fully assemble a chamber built to measure the WVTR inside the glovebox, as shown in **Figure 10a**.

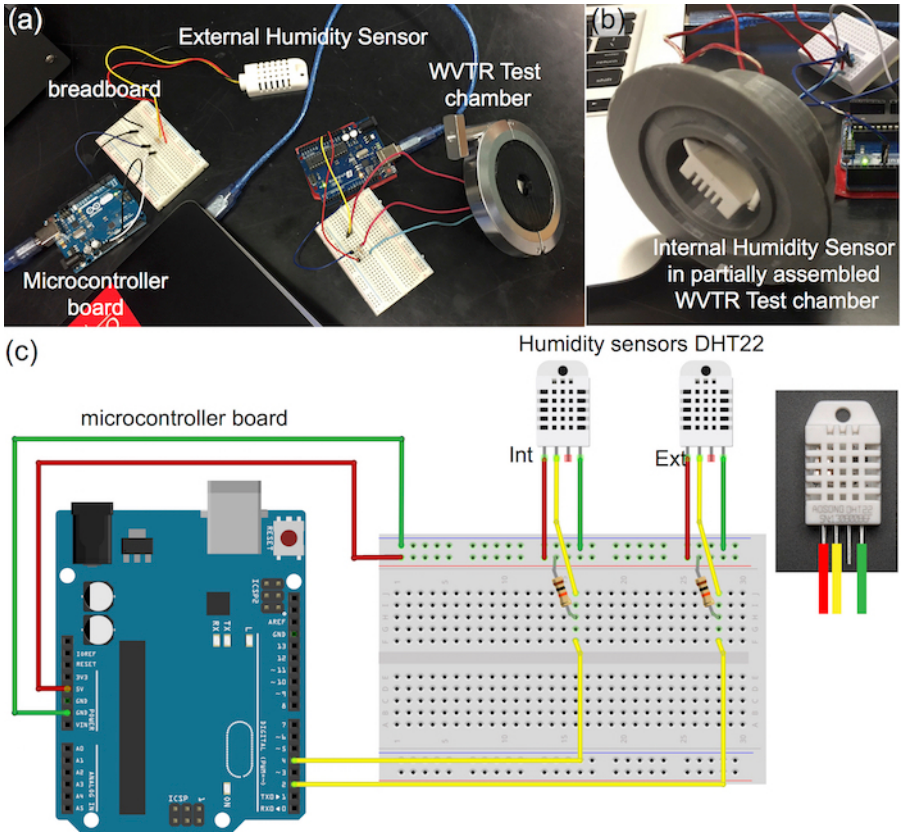

Figure 10: The humidity testing setup. (**a**) This panel shows a completely assembled WVTR test chamber wired to internal and external DHT22 humidity sensors using a breadboard jumper to a microcontroller. (**b**) This panel shows the DHT22 humidity sensor inside the WVTR test bottom chamber. Note that the wires are fed through the bottom chamber and are held in place with low-pressure epoxy. (**c**) This panel shows a schematic of the internal and external humidity sensor DHT22 and a microcontroller board wiring diagram using a single breadboard (for convenience). The sensor is connected to the microcontroller pins "5 V" (red) and "GND" (green) to provide power to the sensor. The data output from the sensor (yellow) connects to the pins in "DIGITAL" [2 for the internal (INT) sensor and 4 for the external (EXT) sensor] with a 10 kΩ resistor. The inset shows a DTH22 sensor with the correct pin wiring: 5V (red), ground (green), and data (yellow). Please click here to view a larger version of this figure.

7. Conduct a Humidity Measurement to Determine the WVTR

1. Download the microcontroller board software and any Python 2.7.12 IDE on a compatible computer.
2. Open Python file **Run_WVTR_Test.py**.
3. Plug in the microcontroller to the computer *via* a USB A-B cable.
4. Install the library to allow the output of the data to a spreadsheet.
5. Repeat step 5.4 to determine the COM number of the connected microcontroller. Copy and paste this into the Python code as shown in **Figure 11a**.
6. Identify desired file path for raw data spreadsheets and enter it into the Python code as shown in **Figure 11a**.
7. Open the microcontroller file **ARDUINO_HUMIDITY_TESTS.ino**.
8. Under the **Tools** tab, select the appropriate microcontroller as the board. Under the **Tools** tab again, select the port as determined in step 7.5.
9. Verify and upload the microcontroller code to the microcontroller by clicking the icon in the top left of the window as seen in **Figure 11b**.
10. Wire the circuit as shown in **Figure 10c**; connect the 5 V (red), ground (black), and signal (yellow) wires of the external (EXT) humidity sensor to their respective locations. Omit the internal sensor (INT) until step 7.12 since it is located in the completed chamber, as shown in **Figure 10b**.
11. Remove the assembled chamber from the glovebox.
12. Immediately wire the internal sensor in the chamber to the microcontroller board as shown in **Figure 10c**.
13. Run the Python script and follow the prompts that appear in the Python shell.
    1. Type in the material of the chamber.
    2. Type in the duration in hours. Bracket the number with an underscore. For example, if 6 h is desired, then type “_6_”.
    Note: The test should begin and create .xlsx files in the path location specified within the script when the test is complete. Do **NOT** allow the sensors to disconnect from the setup. The test must be restarted if this happens. The microcontroller code for the WVTR measurement was adapted from the default program provided by the supplier. The Python code that runs the IV measurement was adapted from the code supplied by the manufacturer of the ZIF test board.

(a)
```
import serial
import os.path
import xlsxwriter
import sys

serial_port = '' #Add serial port ID/COM number of where internal sensor is connected
baud_rate = 9600;


sen = serial.Serial(serial_port, baud_rate)

date = datetime.now().date()

matl1 = raw_input("\nMaterial 1:\t ")
dur = raw_input("\nDuration in hours:\t")

filepath = '' #Desired spreadsheet path goes here
```
Paste COM number/serial port ID here

Paste desired filepath here

(b)
```
#include "DHT.h"

// what pin we're connected to
#define DHTPIN2 2
#define DHTPIN4 4
#define DHTPIN6 6

#define DHTTYPE DHT22   // DHT 22  (AM2302)

DHT dht_ext(DHTPIN2, DHTTYPE);
DHT dht_int1(DHTPIN4, DHTTYPE);
DHT dht_int2(DHTPIN6, DHTTYPE);

//variables

const byte numChars = 32;
char receivedChars[numChars];
boolean newData = false;

int led = 13;
int dur_in_hr;
float time_elaps;

void setup() {
  Serial.begin(9600); //baud rate
  dht_ext.begin();
  dht_int1.begin();
  dht_int2.begin();
  pinMode(led, OUTPUT);
}

void loop() {
```

Figure 11: A water vapor transmission rate screenshot. These panels show (**a**) a screen shot of the **Run_WVTR_Test.py** Python script with (**b**) the COM port location indicated. Please click here to view a larger version of this figure.

Representative Results

Current-voltage Measurements:

This chamber is designed to allow for the testing of an air-sensitive diode device, such as an organic or perovskite solar cell or a light-emitting diode. It can act as a reusable, temporary encapsulation or as a method of introducing contaminants to perform controlled degradation testing. The current density-voltage (JV) curves shown here were measured using a ZIF test board attached to an SMU under dark (*i.e.*, no illumination) and illuminated conditions to extract the basic diode characteristics. By connecting the contact pins from the chamber to the ZIF board, each pixel can be individually addressed. In the example data below, the standard bottom chamber, without the gas ports, printed from 50% density PLA plastic was used to test an organic solar cell using the 6-pixel configuration. In these organic devices, "pixel" refers to the individual diode that can be measured using the measurement setup. Using the provided Python programs in the **IV Measurement Code** folder (found in the **Supplementary Information**), the following curves were attained for a single pixel from organic devices with a device architecture of ITO/ PEDOT: PSS/P3HT: PCBM/Al. The details for producing the devices can be found elsewhere[16].

Figure 12 represents the expected JV curves of one good working organic photovoltaic device in the dark and under illumination. Note that, to extract the current density (J), the current-voltage curves that are the outputs from the **BasicIV.py** Python program were divided by the measured diode area. For our diodes, this was around 1.2 mm^2. **Figure 12** shows the behavior of one diode within the chamber, with good pin contact with the electrode pads. All four pixels that are measurable in such a configuration show similar behavior. A working organic diode that is not degraded should show rectifying behavior, a low signal to noise, and an exponential increase in the current after an applied voltage of around 1 V in dark conditions; under illumination, it should have similar diode characteristics as in the dark, offset by the induced photocurrent[2,16]. For comparison, **Figure 12** also shows the JV curves for one pixel from the same device, encapsulated using a microscope slide over the active area (*i.e.*, the red outline area from **Figure 4**, sealed with low-pressure vacuum-sealing epoxy after the initial in-chamber tests). Notice that in the chamber, there is evidence of higher contact resistance as shown by the decrease of the fill factor[17] [the curve becomes less "square" due to slope around the short circuit current (J_{sc})[18] and the open circuit voltage (V_{oc})][19]. This can be attributed to the higher contact probe resistance of the device in the chamber compared to the device probed directly using the measurement board[20]. It should be possible to decrease the resistance losses significantly through better soldering and wiring designs. In the case of a degraded, non-functioning or poorly contacted organic device, we would not see a diode-like curve, as in **Figure 12c**. Such curves typically have a low measured current, no rectifying behavior, and a high signal-to-noise ratio, indicating "noise" or open contact. A short circuit, such as would occur if there was a direct contact between the top metal electrode and the ITO electrode on the bottom, would be shown by a straight line of a slope proportional to the resistance across the contact (**Figure 12d**).

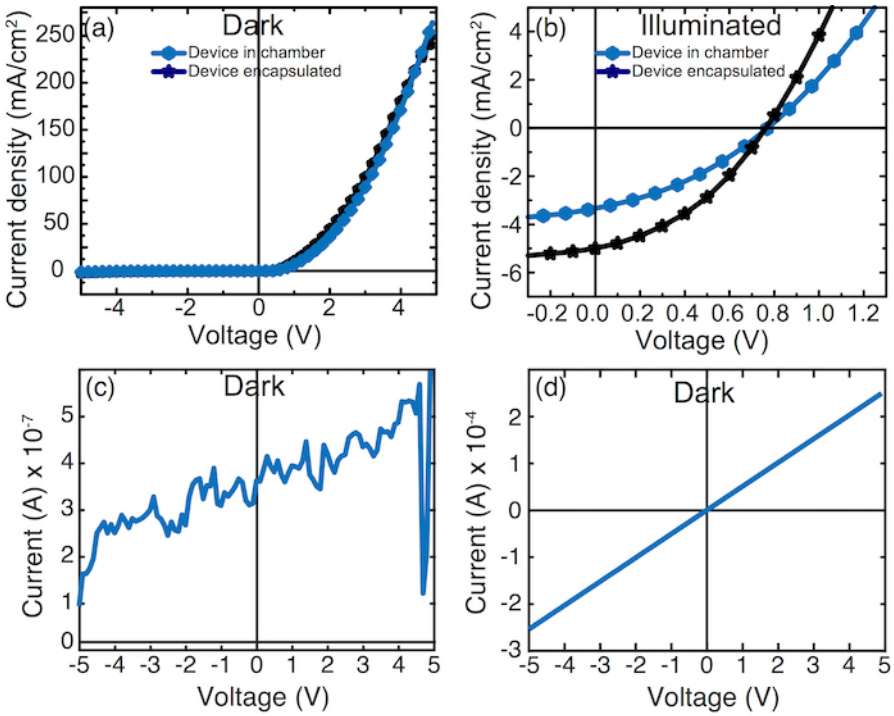

Figure 12: An IV comparison. These panels show the current density-voltage (JV) measurement curves of a standard organic solar cell device inside the chamber and the same device encapsulated and contacted directly to the ZIF board through the built-in pins (**a**) under dark conditions (*i.e.*, not under illumination) and (**b**) under illumination using a lab light source, showing expected diode behavior. (**c**) This panel shows an IV measurement curve of a standard organic solar cell device not under illumination showing degraded or non-contact behavior. (**d**) This panel shows an IV diode measurement curve of a short-circuited device not under illumination. Please click here to view a larger version of this figure.

Chamber Efficacy Tests:

This chamber is intended to act as a temporary, reusable stable environment with controlled properties (including humidity, gas introduction, and temperature). To determine the efficacy of the atmospheric chambers, they were characterized in two ways: a water vapor transmission rate test using a humidity sensor and a device degradation test using the organic solar cell device used to demonstrate the current-voltage measurements in the previous section.

WVTR Tests:

One of the critical factors in the degradation of devices is the penetration of water into the device[21,22]. For long-term device stability, a good encapsulation of organic devices should have 10^{-4} - 10^{-6} g/m^2/day of water ingress[12,13]. As this chamber is designed to be a controlled environment for testing purposes rather than a long-term storage or encapsulation method, the requirements for an effective chamber are not as strict. Rather, the chamber should be able to maintain the device properties within a reasonable timeframe for a given experimental condition. The primary method of characterizing water vapor ingress and the use time of the chamber is the water vapor transmission rate (WVTR)[21].

The WVTR can take different meanings depending on the conditions under which it is measured and the units that are used[23]. For the purpose of this contribution, the WVTR is determined through a measure of relative humidity change[24], similar to a gravimetric cup test[23]. Due to the complexity of the moisture ingress paths in the chamber, the mass change of the water vapor reaching the sensor shall be used, normalized by the per percentage difference (expressed as a fraction from 0 - 1) of the relative humidity across the boundary, adapted from the method of Basha *et al.*[25].

(1) $$WVTR = \frac{\dot{m}}{\Delta RH}$$

Here, $\dot{m}$ represents the rate of change with respect to the time of the mass of water vapor contained in the chamber, and ΔRH is the difference in relative humidity inside and outside the chamber. Such an approach yields units for the WVTR of the mass-per-unit time.

Implicit in this equation is the assumption that the rate of the water vapor ingress is proportional to the relative humidity difference between the inside and the outside of the chamber. This assumption leads to the following differential equation:

(2) $$\frac{dRH_{int}}{dt} + \frac{WVTR}{V\rho}(RH_{int} - RH_{ext}) = 0$$

Here, V is the volume of the chamber (taken from the 3D models), and ρ is the saturation density of the water vapor at the temperature recorded during the test.

Solving this equation and substituting it in the initial condition of 0% humidity in the chamber (ensured by leaving the chamber in the glovebox for > 24 h), the governing equation of these experiments, as shown below, can be found.

(3) $$\ln\left(1 - \frac{RH_{int}}{RH_{ext}}\right) = -\frac{WVTR}{V\rho}\, t$$

When conducting the humidity test, relative humidity readings were taken simultaneously from inside and outside the 3D-printed chamber. Once this data was compiled, it was plotted against time, *t*, as shown in **Figure 13a**. Linear regression was used to calculate the WVTR from the slope of the best fit line.

In this test, 50% print density PLA 3D-printed plastic was used. The test was run for a duration of 4 h, resulting in a WVTR of 270 µg/day (R^2 = 0.985). This is high compared to the requirements for a good organic device encapsulant[12,13], but it is sufficient to minimize the device degradation for an electrical testing lasting several hours[21] (see next section, **Device Degradation Test**). By contrast, a leaking chamber as shown in **Figure 13b** had a WVTR of 855 µg/day (R^2 = 0.99).

The rate at which moisture enters the chamber is governed by the diffusion coefficient of the most permeable material[23]. Assuming the same sealing conditions, different materials for the chamber walls will yield different values of WVTR. Results for a few representative materials and conditions are summarized in **Table 1**. The typical PLA chamber has a higher WVTR than an equivalent chamber machined out of metal[10]. Assuming a proportional relationship between the WVTR and device degradation, we can estimate the storage time before an 80% loss of the initial performance (T80)[6,8] for a test device, using that chamber as a baseline for the moisture ingress of the seals. This can give a rough estimate of the usability time for a chamber in a given configuration. Under such conditions, the 50% density PLA chamber should be able to store a sample without any significant losses for around 3 days. This contrasts with a true encapsulation, where the significant performance was observed after more than two weeks of storage in ambient conditions.

It is also possible to extend the usable time window for a chamber by flowing an inert gas, such as N_2. In such a configuration, the WVTR for the 50% PLA chamber decreased to below the detection limit of the sensor (see **Figure 13b**). With a minimum detection of a ~ 0.1% relative humidity change, that suggests a WVTR of less than 0.13 µg/day, with a significant increase in the estimated storage time. However, previous studies[10,27] have indicated that samples have a T90 of around 6 weeks in a glovebox. As this gas flow chamber configuration is comparable to an inert gas glovebox environment, this is a more likely upper bound for sample storage. To determine a more accurate measure of the WVTR for such low levels of water ingress, a more sensitive test such as the electrical calcium test[28] should be used to give a better estimate.

If further testing of the chambers is desired, an oxygen sensor could be placed in the chamber and the oxygen levels could be monitored over time to give the oxygen transmission rate (OTR), which could be compared with the WVTR.

Material	DRH_{int} (total test duration)	WVTR (mg/day)	Estimated device storage time (days)
50% Density PLA	1.80%	271 ± 30	3.3
50% Density PLA (Leaking)	4.70%	855 ± 90	1
50% Density PLA with N_2 Flow	<0.1%	<0.130	>7000
Water resistant polymer	9.00%	3064 ± 300	0.29
Metal [1]	--	90*	10
* corrected for external relative humidity			
[1] Reese, et al [10]			

Table 1: The results for a few representative materials for the chamber walls and sealing conditions. This table illustrates the total change in internal relative humidity and water vapor transmission rate for chambers of various materials and in various conditions.

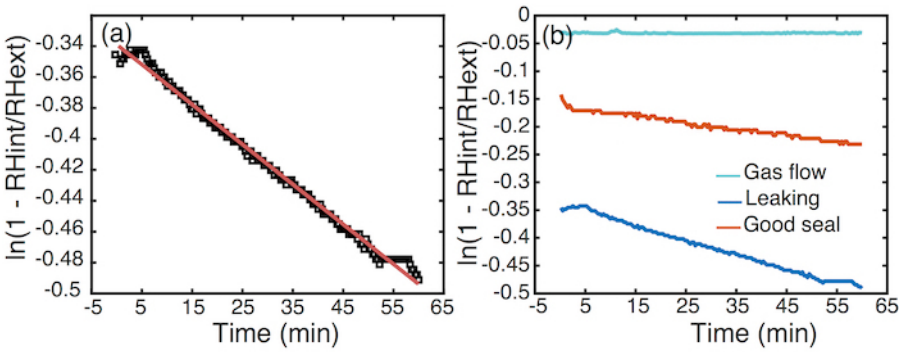

Figure 13: Water vapor transmission rate plots. (**a**) This panel shows a change of relative humidity used to determine the WVTR using equation 3. The dependent variable is the unitless natural logarithm of the ratio of the relative humidity (RH) of the internal and external sensors, plotted against time (see equation 3 in the **Representative Results**). The slope of the reduced square linear regression line is proportional to the WVTR, reported in **Table 1** (R^2 = 0.99). (**b**) This panel shows a change of the relative humidity for a 50% PLA 3D-printed chamber under various conditions. Please click here to view a larger version of this figure.

Device Degradation Test:

To test the degradation in the device performance under continuous operation, diodes were electrically stressed every 5 min from -5 to 5 V, to record the dark current response as a current-voltage curve. **Figure 14** shows a comparison between the change in current at 4 V for a device tested inside the chamber *versus* a standard encapsulated diode. Due to the increased resistance, the device in the chamber has a slightly lower initial current than the encapsulated device. For both devices, an initial increase in the current is observed over the first 50 min period. After a maximum current is attained around 50 - 60 min, there is an inversion in the current curves and the current starts to decrease. This behavior is expected for this type of device, as the formation of a thin oxide interlayer at the top contact electrode initially improves the interface characteristics between the metal and the organic semiconductor[6]. This effect is much more pronounced in the device in the chamber, suggesting greater and faster oxidation. This underscores that the chamber is not intended to be a replacement for the encapsulation for long-term storage, but a portable controlled environment that can be used to measure changing device properties. Adding gas ports with flowing inert gases which decrease the WVTR would likely improve the stability of devices inside the chamber.

As the device is further stressed, the active layer begins to degrade due to a variety of interactions[6,7,8,22]. Both devices show around 0.3 - 0.4 µA/min of loss-of-current as the measurement proceeds, though again, the chamber shows a higher rate of degradation. This underscores that the device inside the measurement chamber is behaving equivalently to the encapsulated device under electrical stress. As shown in **Figure 14**, the decay curves, based on the normalized current change over time, suggests a T80 for continuous use that is similar for the two devices (26 h *vs.* 30 h), though slightly longer for the encapsulated device.

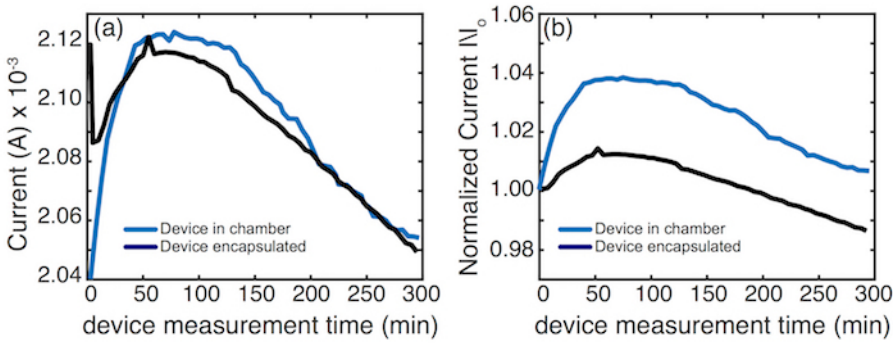

Figure 14: Operational device degradation. (**a**) This panel shows a measured dark current at 4 V for IV measurements taken every 5 min for a standard organic solar cell device. (**b**) This panel shows normalized dark current decay curves at 4 V, I/I_o, where I_o is the initial current. Please click here to view a larger version of this figure.

In the raw data decay curve for the encapsulated organic device (**Figure 14a**), a sharp decline is observed between the first and second measurement over the course of 5 min. This decline is not observed for the organic device tested in the chamber. This is likely a result of the fact that it takes longer to assemble the organic device inside the chamber and attach it to the ZIF board whereas the encapsulated device can be directly measured immediately upon being removed from the glovebox environment.

Discussion

The critical steps in recreating this experiment include the printing of the chambers to avoid cracks, gaps, or poor in-fill characteristics which can decrease the WVTR, sealing the chamber to prevent any ingress of moisture and oxygen by tightening the KF50 clamp to achieve a full sealing between the top and bottom chambers, using a vacuum-rated low-pressure epoxy around the contact pins or any feedthroughs to prevent any leaking, and creating a seal between the sample and the top chamber using a proper O-ring placement and sufficient pressure with the tightening screws on the retaining ring to prevent any leakage without cracking the sample. The O-ring should fit completely into the groove, without burrs or particulates, and should be compressed between 15 - 25% of its cross-section for an adequate seal[10]. It is also important to be careful when attaching the contact pins to the chamber body to both ensure good electrical contact and prevent paths for oxygen and moisture ingress through the low-pressure epoxy. An epoxy rated as a sealant for vacuum applications will provide an adequate seal. It is important to connect the contact pins to the measurement board to minimize any series resistance losses during the IV measurements. Store the chamber in an inert environment such as a glove box for at least 24 h before use to ensure that any moisture absorbed by the chamber has had time to escape from the material. This is especially important if the chamber has been stored for a more than a few days under ambient conditions in the open lab environment. It is not recommended to heat the chamber to accelerate the process of degassing, to avoid a softening of the chamber walls and the risk of collapsing the chamber structure.

Certain common problems can be encountered when recreating this experiment. As the chamber uses an O-ring seal pressed directly onto the tested sample, rather than a completely sealed chamber, it is possible to crack the sample when excessive force is used in mounting the retaining ring. Additionally, particulates on the O-ring or in the groove or burrs on any of the sealing joints can prevent a good seal, in addition to cracking the sample upon mounting[10]. A careful cleaning of the O-ring and the joints before mounting the ring is essential.

It is also important to avoid melting the chamber during the epoxy curing. After applying epoxy to secure the pogo pins in the bottom chamber, refrain from applying heat to speed up the drying process. This will result in melting the 3D-printed material, and hence in a disfiguration of the chamber.

The use of inadequate electrical connections between the contact pins and the test board is a significant problem. A poor solder, long wire connections, or a too thick gauge of wire can lead to a significant, avoidable decrease of the device performance due to resistance losses that occur along the electrical connections between the chamber and the test board. It is advised to always make an encapsulated organic device as a reference to check the quality of the connections outside of the chamber when wiring a new chamber. High resistance losses are likely if the device in the chamber shows orders of magnitude of less dark current or a significant slope around the short circuit current[18] (*i.e.*, I_{sc}, around V = 0) and the open circuit voltage[19] (*i.e.*, V_{oc}, around I = 0). These effects are shown in **Figure 15**, where the use of thick long wires to connect an unsupported chamber to the measurement board is compared to a support collar with embedded interconnects. As can be seen, the use of the support collar led to an increase in the dark current of two orders of magnitude (**Figure 15a**) and to an increase in the fill factor[17] from 22.7% to 34.6%. It may be possible to further decrease the resistance losses through better soldering and wiring designs.

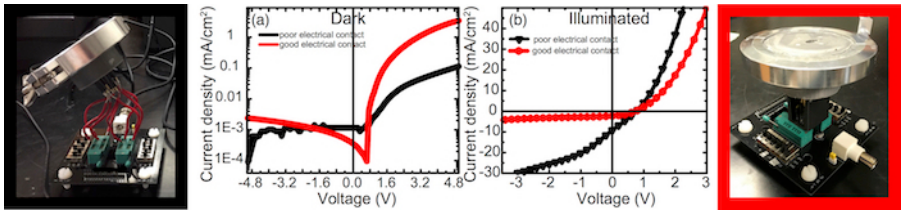

Figure 15: A HiRs IV comparison. These panels show electrical measurements for devices with poor and good contacts: (**a**) dark current-voltage measurements and (**b**) current-voltage measurements under illumination. The inset pictures represent the poor electrical contact configurations (the black border on the left-hand side) and the good electrical contact configurations (the red border on the right-hand side) to connect the contact pins from the chamber to the test measurement board. Please click here to view a larger version of this figure.

The use of a third helping-hand soldering station, clamps, and alligator clips to secure the solder cup and pogo pin will make soldering the contact pins easier, preventing any poor soldering of the contact pins. Ensure that the bead of the solder applied externally to the pin and cup is not too large; otherwise, it will not fit through the embedded holes in the bottom chamber. The solder must be placed on the outside of the pin, as soldering inside will cause the solder to enter the spring and render the pin unusable. Check the electrical connection across the pin and cup by using a multimeter.

When soldering external wires to the DHT22 temperature and humidity sensor, difficulties may be encountered as a result of the precision required due to how narrow the pins are, leading to a poor soldering of the wires to the sensor. Using a third helping-hand soldering station or any clamps and alligator clips will assist in securing the sensor and wires in place. Note that positioning the soldering iron too close to the base of the pin on the sensor for an extended period of time may burn the pin, causing it to fall off.

There are two main limitations to the general approach proposed here of using a 3D-printed atmospheric chamber. The first is that the WVTR is substantially higher for the 50% PLA-printed chamber than it would be for an equivalent chamber machined from metal. Therefore, in order to reduce the WVTR, two modifications exist for the chamber design that can increase the use time of the chamber: flowing inert gas and desiccant wells. To allow the flowing of inert gas, the bottom chamber with the gas ports configuration of the chamber design can be used. The WVTR was substantially decreased to less than 0.13 µg/day in such a configuration. To accommodate desiccants, the bottom chamber has three wells around the feedthrough holes. These wells can be filled with standard moisture or oxygen getters to absorb any gases that enter the chamber. Reese *et al.*[10] found that high-surface-area Getters of mixed Mg and drierite (both standard laboratory desiccants) were sufficient to decrease the WVTR for metal chambers to 0.5 µg/day.

The second limitation is that the chamber, through the use of pogo pins and wiring connections to the measurement board, always shows higher contact resistance losses compared to an equivalent encapsulated device. **Figure 12b** shows this behavior for a device in the chamber compared to the same device encapsulated and contacted directly to the ZIF test board. This may have implications for the interpretation of the device's characteristics. Every effort must be made to limit the losses of this nature through proper wiring and soldering. As shown in **Figure 15**, it is possible to reduce losses significantly by improving the wiring connections between the chamber and the ZIF test board. Using a custom 3D-printed collar embedded with copper wires that fit directly into the ZIF test board, the device performance was improved significantly. Further improvements may be possible with better connection configurations or with other test boards.

An additional limitation is specific to the chamber designs described in this protocol but may be alleviated by researchers adopting designs for their own uses by changing the chamber configurations. Any organic device tested with the chambers as specified by the provided CAD files (as described in **Figure 1**) are limited in size to 40 mm in diameter. The total active area that can be illuminated is also limited by the size of the window in the top chamber. The 6-pixel design requires an oval shape for the top chamber opening which blocks two of the pixels, whereas the 4-pixel design has all pixels exposed within an 18 mm circle.

This protocol outlines an approach to build and test a small portable chamber, based on the original design by Resse *et al.*[10]. We have adapted this design, making it cheaper and more versatile by using 3D printing to produce the chamber components. The significance with respect to other protocols lies in its simplicity, adaptability, and accessibility. The use of 3D printing rather than machining allows for rapid, cost-effective adjustments to changing sample or environmental requirements while maintaining the utility of the basic design. In this contribution, we have proposed three variations of the chamber that can be produced, including different pixel layouts for the organic devices and ingress ports to flow various gases. The low cost and speed of the production using 3D printing can allow researchers to rapidly modify the design to suit their own purposes, including different pixel layouts, scaled device sizes, extra ports, and additional sensors.

The main rationale for using 3D printing for this chamber was to allow for an increased versatility of the chamber design to accommodate the specific needs of the users. This inherently implies that modifications can be easily made to suit a given purpose, from scaling up to a larger organic device or module designs, adding different measurement functionalities, to changing the organic device layout, giving a wide range of future applications. We propose two possible developments that will extend the use of these chambers even further. They include the ability to change the device layout and to control the temperature.

To change the device layout, as demonstrated above for the 4- and 6-pixel chamber configurations shown in **Figure 1** and **Figure 4**, the chamber can be easily adapted to different organic device pixel layouts, using the CAD files available in the **Supplementary Information**. The location of the electrical feedthrough holes in the bottom chamber should be carefully re-designed to accommodate the appropriate organic device configuration. Note that the retaining ring overlaps with the corners of the organic device in order to secure it in the top chamber and, as such, electrical connections should not be placed in those areas. The top chamber has a hole to allow for the absorption/emission of light by the device. Any organic device tested with this chamber is, therefore, limited to active material in a region not outside of this area. The 6-pixel design requires an oval shape for the top chamber opening which blocks two of the pixels, whereas the 4-pixel design has all pixels exposed within an 18 mm circle. Care needs to be taken to ensure that the groove is deep enough to accommodate a new O-ring if necessary. Reese *et al.*[10] indicate that the O-ring should be compressed between 15 - 25% of its cross-section for an adequate seal. Some CAD files for the top and

bottom chambers without a specific design are also included in the **Supplementary Information** to aid any researcher in developing their own design.

As the chamber design is based on a standard vacuum fitting-a KF50-centering gasket-to ensure a good seal between the top and bottom chambers, it is well suited to accommodate devices smaller than 40 mm in diameter. Scaling up to larger sizes is possible, using other commercially available vacuum flange configurations such as the ISO series, which uses the same centering gasket design. Using a commercially available seal which is tested and certified makes it easy to repeatedly reassemble the chamber without any concern for the integrity of the seal[10]. If the design is to be changed to incorporate more space, be aware that increasing the size of the chamber also increases the transmission of water vapor and oxygen.

Any testing of the organic devices generally does not incorporate temperature control during the IV characterization[14]. As the organic device performance and stability is highly dependent upon the temperature[6,7,8], this can lead to a significant problem in the comparability and reproducibility of reported laboratory test results[14]. Attempts to establish standard testing protocols for organic devices[29,30] suggest that a temperature measurement and control should be built into any electronic test configuration. To address this problem, the atmospheric chambers have two modifications.

The first, a thermocouple probe feedthrough, is already implemented in the available designs as an additional contact pin at the center of the device (see the blue dots in **Figure 4**). Though it is placed at the center to minimize inaccuracies in pixel-to-pixel temperature readings from gradients across the device, the thermocouple may also be moved into the retaining ring so as not to interfere with the electrical measurements. The low thermal conductivity of PLA means that such a modification may require the use of metal for the retaining ring.

The second, for a method to control the temperature, is a thermoelectric cooling/heating ring applied to the top chamber. The ceramic cartridge heating/cooling ring can be applied to the exterior of the top chamber to emit or dissipate heat, as shown in **Figure 16**. The ring can be used for heating or cooling simply by reversing the side placed on the chamber. Due to the low thermal conductivity of PLA, this method is only effective for a highly thermally conductive top chamber material, such as metal.

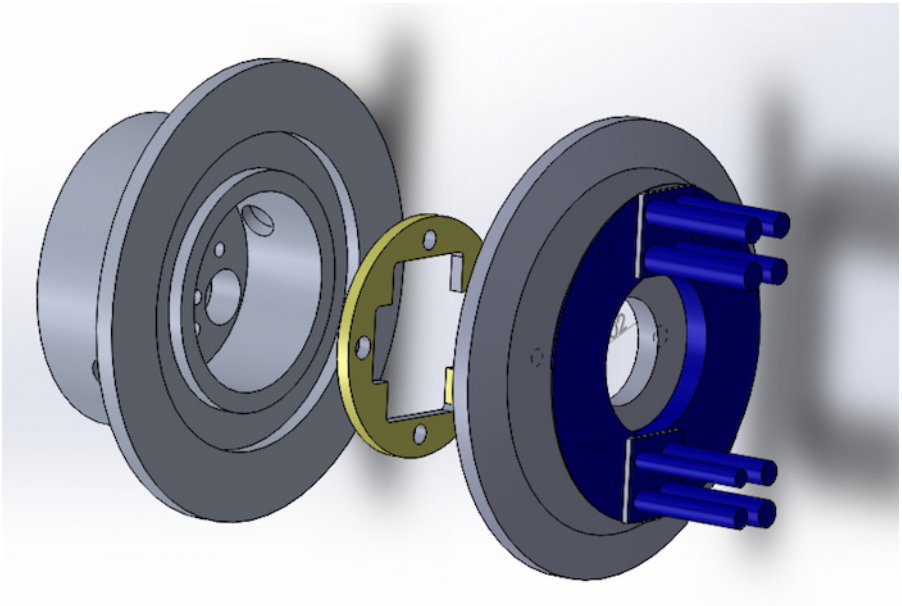

Figure 16: An exploded view of the chamber with cooling. This panel shows an exploded view of a test chamber assembly with a cooling ring and the heat sink placement shown in blue. Note that for an optimal performance, the rod heat sinks should be placed all around the diameter of the ring, not just the two shown here for clarity. Please click here to view a larger version of this figure.

To dissipate heat effectively, a heat sink and fan must also be used during the operation. For an optimum performance, the heat sinks should be placed around the cooling ring to maximize the covered area. Any fan can be used, though stronger fans will provide a better performance. The application of the cooling ring and heat sinks can be done with a thermally conductive epoxy. While most epoxy can be removed with acetone, make sure the epoxy can be removed from the heat sinks and ring prior to the application if heating is required.

Disclosures

The authors have nothing to disclose.

Acknowledgements

The authors acknowledge Peter Jonosson and the Lyons New Media Centre for the 3D printing of the chambers. This research was supported by 436100-2013 RGPIN, ER15-11-123, the McMaster Dean of Engineering Excellence Undergraduate Summer Research Award, and the Undergraduate Research Opportunities Program.

References

1. Tremblay, J.-F. The rise of OLED displays. *Chemical & Engineering News.* **94** (28), 30-34 (2016).
2. Kang, H. *et al.* Bulk-Heterojunction Organic Solar Cells: Five Core Technologies for Their Commercialization. *Advanced Materials.* **28** (36), 7821-7861 (2016).
3. Jacoby, M. The future of low-cost solar cells. *Chemical & Engineering News.* **94** (18), 30-35 (2016).
4. Veldhuis, S.A. *et al.* Perovskite Materials for Light-Emitting Diodes and Lasers. *Advanced Materials.* **28** (32), 6804-6834 (2016).
5. Park, N.-G. Perovskite solar cells: an emerging photovoltaic technology. *Materials Today.* **18** (2), 65-72 (2015).
6. Turak, A. Interfacial degradation in organic optoelectronics. *RSC Advances.* **3** (18), 6188 (2013).
7. Scholz, S., Kondakov, D., Lüssem, B., Leo, K. Degradation Mechanisms and Reactions in Organic Light-Emitting Devices. *Chemical Reviews.* **115** (16), 8449-8503 (2015).
8. Jørgensen, M., Norrman, K., Gevorgyan, S.A., Tromholt, T., Andreasen, B., Krebs, F.C. Stability of Polymer Solar Cells. *Advanced Materials.* **24** (5), 580-612 (2012).
9. Habisreutinger, S.N., McMeekin, D.P., Snaith, H.J., Nicholas, R.J. Research Update: Strategies for improving the stability of perovskite solar cells. *APL Materials.* **4** (9), 091503 (2016).
10. Reese, M.O., Sigdel, A.K., Berry, J.J., Ginley, D.S., Shaheen, S.E. A simple miniature controlled-atmosphere chamber for optoelectronic characterizations. *Solar Energy Materials and Solar Cells.* **94** (7), 1254-1258 (2010).
11. Gevorgyan, S.A., Jorgensen, M., Krebs, F.C. A setup for studying stability and degradation of polymer solar cells. *Solar Energy Materials and Solar Cells.* **92** (7), 736-745 (2008).
12. Park, J.-S.S., Chae, H., Chung, H.K., Lee, S.I. Thin film encapsulation for flexible AM-OLED: a review. *Semiconductor Science and Technology.* **26** (3), 034001 (2011).
13. Ahmad, J., Bazaka, K., Anderson, L.J., White, R.D., Jacob, M.V. Materials and methods for encapsulation of OPV: A review. *Renewable & Sustainable Energy Reviews.* **27**, 104-117 (2013).
14. Gevorgyan, S.A. *et al.* Round robin performance testing of organic photovoltaic devices. *Renewable Energy.* **63**, 376-387 (2014).
15. Osterwald, C.R., Hammond, R., Zerlaut, G., D'Aiello, R. Photovoltaic module certification and laboratory accreditation criteria development. *Solar Energy Materials and Solar Cells.* **41**, 629-636 (1996).
16. Turak, A. *et al.* Systematic analysis of processing parameters on the ordering and performance of working poly(3-hexyl-thiophene):[6,6]-phenyl C(61)-butyric acid methyl ester solar cells. *Journal of Renewable and Sustainable Energy.* **2** (5), 53103 (2010).
17. Qi, B., Wang, J. Fill factor in organic solar cells. *Physical Chemistry Chemical Physics.* **15** (23), 8972-8982 (2013).
18. Lu, N., Li, L., Sun, P., Liu, M. Short-circuit current model of organic solar cells. *Chemical Physics Letters.* **614**, 27-30 (2014).
19. Qi, B., Wang, J. Open-circuit voltage in organic solar cells. *Journal of Materials Chemistry.* **22** (46), 24315-24325 (2012).
20. Xue, J., Uchida, S., Rand, B.P., Forrest, S.R. 4.2% efficient organic photovoltaic cells with low series resistances. *Applied Physics Letters.* **84** (16), 3013-3015 (2004).
21. Hauch, J.A., Schilinsky, P., Choulis, S.A., Rajoelson, S., Brabec, C.J. The impact of water vapor transmission rate on the lifetime of flexible polymer solar cells. *Applied Physics Letters.* **93** (10), 103306 (2008).
22. Norrman, K., Madsen, M.V., Gevorgyan, S.A., Krebs, F.C. Degradation Patterns in Water and Oxygen of an Inverted Polymer Solar Cell. *Journal of the American Chemical Society.* **132** (47), 16883-16892 (2010).
23. Dameron, A.A., Reese, M.O., Moriconie, T.J., Kempe, M.D. Understanding Moisture Ingress and Packaging Requirements for Photovoltaic Modules. *Photovoltaics International.* **5** (August), 121-130 (2009).
24. ASTM E398-13. *Standard Test Method for Water Vapor Transmission Rate of Sheet Materials Using Dynamic Relative Humidity Measurement.* https://www.astm.org/Standards/E398 (2013).
25. Basha, R.K., Konno, K., Kani, H., Kimura, T. Water Vapor Transmission Rate of Biomass Based Film Materials. *Engineering in Agriculture, Environment and Food.* **4** (2), 37-42 (2011).
26. Kim, N. *et al.* A correlation study between barrier film performance and shelf lifetime of encapsulated organic solar cells. *Solar Energy Materials and Solar Cells.* **101**, 140-146 (2012).
27. Reese, M.O. *et al.* Pathways for the degradation of organic photovoltaic P3HT: PCBM based devices. *Solar Energy Materials and Solar Cells.* **92** (7), 746-752 (2008).
28. Kempe, M.D., Reese, M.O., Dameron, A.A. Evaluation of the sensitivity limits of water vapor transmission rate measurements using electrical calcium test. *Review of Scientific Instruments.* **84** (2), 025109 (2013).
29. Reese, M.O. *et al.* Consensus stability testing protocols for organic photovoltaic materials and devices. *Solar Energy Materials and Solar Cells.* **95** (5), 1253-1267 (2011).
30. Castro, F. *Current landscape of standardisation efforts in organic and printed electronics 2015 - a VAMAS review.* https://www.researchgate.net/publication/278035615_Current_landscape_of_standardisation_efforts_in_organic_and_printed_electronics_2015_-_a_VAMAS_review. National Physical Laboratory (2015).

